

Date of publication xxxx 00, 0000, date of current version xxxx 00, 0000.

Digital Object Identifier 10.1109/ACCESS.2017.Doi Number

A block ramp errors correction method of Planet subpixel offset: application to the 2018 Mw 7.5 Palu earthquake, Indonesia

Zhixiong Feng^{1,2}, Guangcai Feng^{1,2}, Huang Chen^{1,2}, Wenbin Xu^{1,2}, Zhiwei Li^{1,2}, Lijia He^{1,2} and Zhengyong Ren^{1,2}

¹School of Geoscience and Info-Physics Engineering, Central South University, Changsha, China

²Key Laboratory of Metallogenic Prediction of Nonferrous Metals and Geological Environment Monitoring (Central South University), Ministry of Education, China

Corresponding author: Guangcai Feng (e-mail: fredgps@csu.edu.cn) and Huang Chen (e-mail: csuchenhuang@csu.edu.cn).

This work is supported jointly by the National Natural Science Foundation of China (No. 41574005, 41574120) and Shenghua Yuying fund of Central South University.

ABSTRACT Planet optical images have a short revisit period and high spatial resolution, so they have great potential in surface offset monitoring. However, few studies have focused on the error source analysis and accuracy improvement in the offset field of Planet images. In this study, we investigate the optimal band selection of the Planet images and the error sources for subpixel offset monitoring, using the 28 Sept. 2018 Mw7.5 Palu earthquake as an example. The results show that Band 2 is the optimal band for surface offset monitoring and ramp errors are the dominating error source in the offset field. Considering the imaging characteristics of Planet satellites, we propose a block ramp errors correction method. Our proposed method can improve the accuracy of the Planet subpixel offset by 25% in comparison with the traditional method. We also compare the Planet images subpixel offset result with the Sentinel-2 subpixel offset result and find they are in good consistency. We combine the corrected Planet images offset and SAR images offset to solve the complete 3D deformation field of the Palu earthquake, which shows that the ruptured fault is a left-lateral strike-slip fault accommodated with normal component in the Palu-Koro fault. The earthquake was dominated by south-north and vertical deformation, with the maximum deformation of 6 m and 4 m in the horizontal and vertical directions, respectively. This study also has set a good example for using the Planet images for natural hazards monitoring (such as earthquakes and landslides).

INDEX TERMS Planet optical imagery, Sentinel-2 optical imagery, Ramp errors, Palu earthquake, 3D coseismic deformation.

I. INTRODUCTION

Despite being vulnerable to cloud and rain, optical imagery is widely used for the emergency response and disaster assessment of large earthquakes and landslides, as it has clear texture features, massive archived data, wide satellite distribution and rapid response [1]. Since its successful application in coseismic deformation mapping of the Mw7.3 Landers earthquake in 1992 [2], the optical imagery and subpixel cross-correlation technology has become an important method for monitoring coseismic deformation. After the COSI-Corr software came out [3], the subpixel cross-correlation technology got significant improvement and has been applied in many large earthquakes [4, 5, 6].

Many studies on the coseismic deformation monitoring used optical imagery, like SPOT, ASTER, HiRISE, Landsat8, Sentinel-2A/B and air photos [7], but few studies considered the systematic errors and influencing factors of using the Planet optical images for deformation monitoring.

Planet is one of the world's largest satellite companies, which has more than 140 satellites in orbit. Every Planet Scope satellite is a cubesat with a size of about 10 cm × 10 cm × 30 cm, which is called "dove" [7]. Compared with Landsat8 and Sentinel-2 images, Planet images have higher spatial resolution (3 m) and shorter revisit period (up to 1 day). The specific satellite parameters are shown in Table 1.

[Insert Table 1 about here]

Different from push-broom sensors like Landsat8, Sentinel-2, ASTER, and SPOT, the Planet satellites obtain frame images [7], and have lighter weight, smaller imaging coverage and more complex orbit control. Therefore, its systematic errors and surface offset correction methods are significantly different from those of push-broom satellites. Therefore, a new algorithm is needed for correcting the offset errors of Planet images.

On 28 Sept. 2018, an Mw7.5 earthquake struck Central Sulawesi Island in Indonesia, which is the largest earthquake in the region since 2005 [8]. Landsat8, Sentinel-2, Planet and SAR images have been applied to acquire the surface deformation of the earthquake in current studies, but these studies do not introduce the correction method of the systematic errors after mosaic the Planet images. And the Planet satellites also have a good image coverage for this earthquake. Therefore, this earthquake is a perfect chance to validate the capability of our method to correct the errors in the Planet images offset field.

In this study, we firstly analyze the subpixel offsets of multiple pairs and conclude the main systematic errors in the offset fields of Planet images. Then we choose the optimal band from the four bands of Planet images for surface offset measurement. Considering the features of Planet imaging mode, we propose a block ramp errors correction method to correct the ramp errors of the Planet subpixel offset. We assess the accuracy and reliability of the Planet subpixel offset by comparing with the result from the Sentinel-2 images. Combining the corrected Planet images offset and ALOS2/PALSAR images offset, we use the weighted least squares method to estimate a complete 3D coseismic deformation field, which can provide a comprehensive deformation interpretation for 2018 Mw7.5 Palu earthquake. Finally, we discuss the error sources in the Planet subpixel offset, the accuracy and the application of the Planet images in surface deformation measurement.

II. ERRORS ANALYSIS AND THE BLOCK RAMP ERRORS CORRECTION METHOD

The error components of optical image subpixel offset are strongly related to optical sensors and imaging mode. Planet satellites data are frame images, and every image is acquired synchronously with the same parameters [7]. So the error composition in the offset field of the Planet images is completely different from that of the push-broom optical images such as Landsat8 and Sentinel-2. We chose the 2018 Mw 7.5 Palu earthquake as an example to analyze its systematic errors components (please see the section III for detail study area introduction). In order to obtain enough samples for analyzing systematic errors, five images acquired before the earthquake (Table 2) by Planet satellites were selected and processed according to the following processing

flow (1)-(3). We obtained 6 pairs of image offsets in east-west (E/W) and north-south (N/S) directions, as shown in Fig. 1.

[Insert Fig. 1 about here]

In Fig. 1, long-wavelength ramp errors and decorrelation noises are more obvious than other errors. There are no stripe artifacts and satellite attitude distortions, which are common in the push-broom satellite images. Therefore, Planet images have great advantages and potential in surface offset monitoring. However, due to the small coverage of each Planet Scope satellite, monitoring one earthquake usually needs a couple of Planet Scope satellites working together. The position difference of satellites and data processing would cause some systematic errors. Even the images acquired by the same satellite, but they have large ground reflection differences at different time, leading to gaps in the mosaicked image. To solve this problem, we propose a new data processing method for the Planet images, which have the following four steps (Fig. 2):

(1) Data pre-processing: Mosaic Planet images over the study area to get a complete coverage. Get the coordinates of the four corners of each Planet image and mosaic the master and slave images. In addition, the master and slave data coverage may not in the same range, so we should choose the data of the same geographical coverage.

(2) Cross-correlation calculation: The data provided by the Planet Company have been done the geometric correction, radiometric correction and orthorectification before being released [9], so we can calculate the cross-correlation directly by the COSI-Corr software [10] and get the E/W offset, N/S offset and signal noise ratio (SNR).

(3) Coordinate conversion: For data fusion and surface deformation interpretation, we transform the offset field from the UTM coordinate system to the WGS-84 coordinate system.

(4) Systematic errors removal: There are decorrelation noises and long-wavelength ramp errors in both the E/W and N/S offset fields. We mask the decorrelation areas to reduce the effects of decorrelation noises. The long-wavelength ramp errors of optical images offset field are mainly resulted from translation and rotation among the input images [11]. In this study, we use polynomial fitting to correct long-wavelength ramp errors for every Planet coverage. The Planet offset field is usually obtained by mosaicking images from different satellites, which would lead to different ramp errors patterns in different planet footprint coverage (see Figs. 4(a) and 4(e)). The traditional polynomial fitting method for the whole image is no longer applicable for this case. We propose a novel method to correct the long-wavelength ramp errors. Specifically, we first segment the subpixel offset obtained in step (3) by the corner coordinates of the Planet images obtained in step (1). Next, we correct the long-wavelength ramp errors from the segmented subpixel offset field using the traditional polynomial fitting model and then synthesize those corrected segmented subpixel offset field into a complete result. Finally, the NL-means filter [12] method is used to further reduce the noise in the offset field.

[Insert Fig. 2 about here]

III. EXPERIMENT AND DATA PROCESSING

A. STUDY AREA AND IMAGE COVERAGE

On 28 Sept. 2018, an Mw7.5 earthquake occurred in Sulawesi, Indonesia. Sulawesi is located at the junction of three plates of Sunda, Australia and Philippine Sea. This earthquake occurred on the NNW Palu-Koro strike-slip fault (PKF) [8, 13, 14], and triggered landslides and tsunamis [15]. According to USGS [16], the epicenter of the earthquake is at 119.94° E, 0.59° S, with a depth of 12 km. This earthquake caused a significant surface slip, which is a good case for the optical images monitoring experiment. We selected the Planet satellite images (spatial resolution of 3 m) and ascending ALOS2/PALSAR images (spatial resolution of 3-10 m, observation range of 50-70 km) as the experimental data (as shown in Fig. 3). The pre- and post-seismic optical and SAR data are shown in Table 2.

[Insert Fig. 3 about here]

B. THE OPTIMAL BAND OF PLANET IMAGES FOR SURFACE OFFSET MONITORING

Although the four bands (Blue: 455-515 nm, Green: 500-590 nm, Red: 590-670 nm, NIR: 780-860 nm) of Planet images have the same spatial resolution (3 m), they have different band width and cause different ground reflectivity errors, especially in the vegetation area [18]. So the four bands would obtain image offsets with different accuracies. We tried to choose the optimal band of Planet images by statistical analysis of the no deformation area for surface offset measurement. Five images acquired before the 2018 Mw 7.5 Palu earthquake were selected for the cross-correlation calculation, and a total of three offset fields were obtained (see Table 3). The specific Planet images acquisition time is shown in Table 2.

[Insert Table 2 about here]

Since the study area was stable before this event, we used the standard deviation of the offset field of different bands to show the ability of offset monitoring of different bands. The specific parameters of the COSI-Corr software for the cross-correlation calculation are as follows: in the frequency domain, the initial sliding window and final sliding window are 32×32 ($96\text{ m} \times 96\text{ m}$) pixels, sliding step size 1 pixel (3 m), iteration 2 times, and mask threshold of 0.95. After removing the systematic errors in the offset field, we further processed it with the NL-means filter. The results are listed in Table 3.

[Insert Table 3 about here]

The error levels of Band 1 and Band 3 are very close. Band 4 has the highest error level. Band 2 has the lowest error level, which is resulted from the largest band width (500-590 nm).

Therefore, in the following, we selected Band 2 of the Planet optical images for the further experiments.

C. PLANET DATA PROCESSING

The specific parameters of the COSI-Corr software for the cross-correlation calculation and NL-means filter are shown in Table 4. The result obtained by the block ramp errors correction method (referred to as the block method hereafter) is compared with the results of the traditional full-field ramp errors correction method (referred to as the full-field method hereafter) (Fig. 4).

[Insert Fig. 4 about here]

In the original offset fields (Figs. 4(a) and 4(e)), there are long-wavelength ramp errors in the offset fields. After correcting the ramp errors, area B in Fig. 4(b) shows larger errors than that in Fig. 4(c), demonstrating that the proposed block method performs better than the full-field method. The proposed method even removed some mosaic errors.

We selected area A of Figs. 4(b), 4(c), 4(f) and 4(g), which is a stable region in the E/W and N/S offset fields of the Planet images, to evaluate the accuracy of the offset results processed by the full-field method and the block method. The standard deviation of this area represents the systematic errors of the whole scene image. As the error histogram (Fig. 5) shows, the mean error and standard deviation of the proposed block method are smaller than that of the full-field method. In addition, there are two peaks in the E/W and N/S error histograms of the full-field method (Figs. 5(a) and 5(b)). The block method can remove the peak caused by ramp errors (Figs. 5(c) and 5(d)).

[Insert Fig. 5 about here]

D. CROSS-VALIDATION OF SENTINEL-2 AND PLANET SUBPIXEL OFFSET

In order to verify the reliability of the Planet subpixel offset result, we used the Sentinel-2 observation for cross-validation, since there are few geodetic measurements (such as leveling and GPS surveying results) available. The Sentinel-2 data were processed by four steps: data pre-processing, cross-correlation calculation, coordinate conversion and errors removal [19]. The Sentinel-2 offset field has decorrelation noises, long-wavelength ramp errors, stripe artifacts and satellite attitude distortions, etc. After removing these errors, the offset field was processed by the NL-means filter. The COSI-Corr and NL-means filter parameters are also shown in Table 4. The comparison between the results of Planet and Sentinel-2 are shown in Fig. 6.

[Insert Table 4 about here]

[Insert Fig. 6 about here]

The Sentinel-2 offset field is smoother than that of the Planet images offset field. The reason could be that the window sizes for the Planet images (initial sliding window: $192\text{ m} \times 192\text{ m}$;

final sliding window: $96 \text{ m} \times 96 \text{ m}$) is smaller than that of Sentinel-2 (Initial sliding window: $320 \text{ m} \times 320 \text{ m}$. Final sliding window: $320 \text{ m} \times 320 \text{ m}$) when we used COSI-Corr for cross-correlation calculation. Bigger window size leads to smoother results. The residual map Figs. 6(c) and 6(f) show the coseismic offset fields observed by these two independent optical satellites have a good consistency. Therefore, the reliability of the subpixel offset results of the Planet images is confirmed.

E. ALOS2 OFFSET-TRACKING RESULT

The SAR image offset-tracking technology has slightly lower accuracy (meter level) than that of InSAR technology (decimeter level), but it can better resist the influence of temporal and spatial decorrelation and does not need phase unwrapping, especially in the near field region with large deformation. We utilized the pixel offset-tracking method to calculate the azimuth and range deformations of ALOS2/PALSAR data for this earthquake with the Gamma software [20]. The calculation window is 50×100 pixels (range \times azimuth), and the range and azimuth step sizes are 5 and 10 pixels, respectively. Finally, the orbital errors in the deformation field were removed, and the azimuth and range deformations were obtained. The azimuth and range deformation results are shown in Fig. 7.

[Insert Fig. 7 about here]

IV. THE 3D COSEISMIC DEFORMATION OF THE PALU EARTHQUAKE

Using the optical images, we can only get horizontal offset. Due to the polar orbital flight of SAR satellites, the ascending or descending orbits can provide range (Line of Sight (LOS)) measurement with high accuracy [21], but N/S measurement with low accuracy. We combined the horizontal offset from Planet images and the azimuth and range offsets from the ascending strip map ALOS2/PALSAR SAR images, to derive the complete 3D deformation of the Mw 7.5 Palu earthquake. We projected the azimuth and range deformations to the E/W, N/S and vertical directions by

$$P \begin{bmatrix} 1 & 0 & 0 \\ 0 & 1 & 0 \\ -\sin\alpha\cos\beta & \sin\alpha\sin\beta & \cos\alpha \\ \sin\beta & \cos\beta & 0 \end{bmatrix} \begin{bmatrix} x \\ y \\ z \end{bmatrix} = P \begin{bmatrix} d_{ew} \\ d_{ns} \\ d_{ran} \\ d_{azo} \end{bmatrix} \quad (1)$$

where α and β represent the incident angle and azimuth angle of the SAR sensors, respectively. x, y and z are the E/W, N/S and vertical deformations, respectively. $P = \text{diag}(\frac{p_1}{p_1+p_2+p_3+p_4}, \frac{p_2}{p_1+p_2+p_3+p_4}, \frac{p_3}{p_1+p_2+p_3+p_4}, \frac{p_4}{p_1+p_2+p_3+p_4})$ is the weight matrix. We used the variance-covariance structure function to determine the weight [22]. First, we selected a region with small deformation as the weighted region. Then we removed the outliers of the region, such as NaN values and larger deformation values, according to the ' 3σ criterion'. Finally, the reciprocal of the variance of the region can represent the weight, that is $p_i = \frac{1}{\sigma_i^2}$ ($i =$

$1, 2, 3, 4$). d_{ew}, d_{ns}, d_{ran} and d_{azo} are E/W, N/S, range and azimuth deformations, respectively.

Equation (1) can be written as a matrix,

$$PBX = PD \quad (2)$$

We calculated Equation (2) by the weighted least squares method to obtain the 3D deformation fields x, y and z . Because the offset result of the optical images and SAR images have different resolutions, we resampled them to the same resolution and coverage for the joint calculation. Then we combined the optical image offset and the SAR image offset to calculate the E/W, N/S and vertical deformations with the optical image E/W weight 0.34, the N/S weight 0.13, the SAR image azimuth weight 0.08 and the range weight 0.45. The 3D deformation results are shown in Fig. 8.

[Insert Fig. 8 about here]

As Fig. 8 shows, the surface deformation of the 2018 Mw7.5 Palu earthquake is dominated by the N/S left-lateral strike-slip and vertical subsidence of normal fault. The rupture of this earthquake is a new fault, which hasn't been recorded [13]. The near field maximum deformation in the N/S direction is about 6 m, which is similar to Song's Landsat8 results [14]. The N/S deformation on the two sides of the PKF is not symmetrically distributed, and the hanging wall fault (East) is significantly larger than that of the footwall (West). This indicates that the earthquake fault inclines to the east. In the vertical direction, the surface subsidence mainly occurs on the hanging wall of the fault. The surface subsidence, up to 4 m, mainly occurred in two areas, areas B and C of Fig. 8(c). The 2018 Mw 7.5 Palu earthquake triggered several landslides, which are also shown in the Planet images offset field (Area A of Fig. 8(a)). The landslide is dominated by the E/W offset, with the maximum offset in the west exceeding 15 m (Figs. 9(c) and 9(f)). This is contrary to the offset characteristics of the earthquake.

[Insert Fig. 9 about here]

V. DISCUSSION AND CONCLUSIONS

Different optical satellite sensors and imaging modes lead to different errors in the offset field. Many studies have discussed the sources and removal methods of the system errors of optical satellites, such as SPOT [23], ASTER [24], Landsat8 [25] and Sentinel-2 [19]. However, these methods cannot be applied to the Planet images, which are frame images. The Planet subpixel offset of the 2018 Mw 7.5 Palu earthquake has mainly decorrelation noises and long-wavelength ramp errors. Unlike the results of push-broom optical satellites (Landsat8 and Sentinel-2), Planet images offset field has no stripe artifacts and satellite attitude distortions. However, they have small coverage of the Planet images, so images from different Planet Scope satellites are needed to monitor a wide range of deformation. But different imaging geometry of adjacent Planet satellites would lead to different long-wavelength ramp

errors patterns in different Planet Scope coverage. Traditional ramp errors correction methods for push-broom optical satellites are no longer applicable. So this study proposed a block method. Note that, Planet images have high spatial resolutions, so if the resolution of the DEM used for orthorectification is two times lower, the topographic artifacts cannot be neglected [26]. The study area is flat, so the topographic signature is not obvious. However, how to reduce the influence of topographic artifacts still needs further research.

The theoretical accuracy of the image offset calculated by the subpixel correlation method is about 1/20-1/50 pixel [24, 27, 28], but the real accuracy of the optical image offset is usually affected by lots of factors, such as post-processing methods. In this study, we correct the coseismic deformation of the 2018 Palu earthquake by the full-field method and the proposed block method, and got accuracies of 0.63 m (0.2 pixel) and 0.45 m (0.15 pixel), respectively. The accuracy level of the traditional method is close to that of the Kääb et al. [7], which studied the offset of the 2016 Mw 7.8 Kaikoura earthquake in New Zealand. The proposed method got a higher accuracy, confirming that the block method can improve the accuracy of Planet subpixel offset. There are also other influencing factors of the accuracy, such as the satellite spatial resolution, sun illumination conditions, temporal and spatial baseline of images. Some studies measured the image offset accuracy using other images. For example, Feng et al. achieved an accuracy of about 0.6 m using the Landsat8 images [22], and Stumpf et al. got an accuracy of about 0.6 m using the Sentinel-2 images [11]. Although the Landsat8 (15 m) and Sentinel-2 (10 m) images have lower spatial resolution than the Planet images (3 m), they can achieve very similar accuracy with Planet images. This is because the study area in [22] and [11] have more favorable weather and sun illumination conditions.

Planet satellites started to provide data since 2009, and with a revisit period of 1 day. It can timely monitor natural hazards such as earthquakes and landslides. In addition, the large number of Planet satellites provide a large amount of archived data, which enables to obtain the time series of surface deformations such as glaciers, landslides and sand dunes. Planet images have small spatial coverage, so they have great advantages in monitoring small range deformation such as landslides. However, for large scale surface deformation monitoring, such as dune migration, selecting the reference area for correcting the ramp errors is difficult. The Landsat8 and Sentinel-2 have a large coverage, so they are more suitable for monitoring large area deformation.

In this study, we proposed a block method. We compared the proposed method with the full-field method, and found that the proposed method can better correct the ramp errors in the offset field. We also evaluated the accuracy of the Planet images offset field in the 2018 Palu earthquake, which is 0.12 m in the E/W direction (mean) with a standard deviation of 0.45 m, and -0.02 m in the N/S direction (mean) with a

standard deviation of 0.45 m. We established the 3D surface deformation field of the 2018 Palu earthquake by combining the offset field of the Planet optical image and the ALOS2/PALSAR image. The 3D deformation field shows that the earthquake mainly ruptured in the PKF, which is a left-lateral strike-slip with normal component fault. The surface deformation caused by the earthquake mainly appears in the N/S and the vertical direction. In addition, we successfully monitored the landslides using the Planet images, which slid westward, with a maximum offset of more than 15 m. Planet images have high resolution and short revisit period, which can serve as a data platform for the coseismic deformation monitoring and post-disaster rescue.

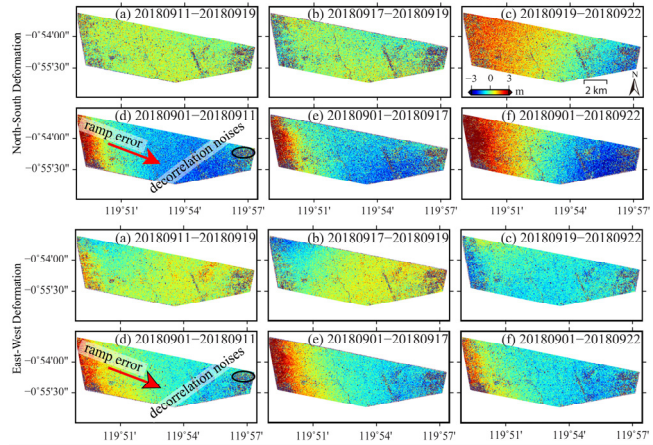


Fig. 1 Error components of Planet images in the E/W and N/S offset fields.

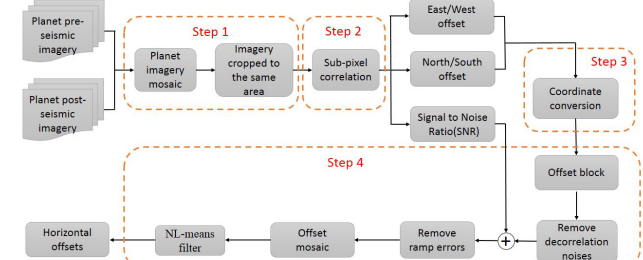


Fig. 2 Processing flow chart of the Planet images.

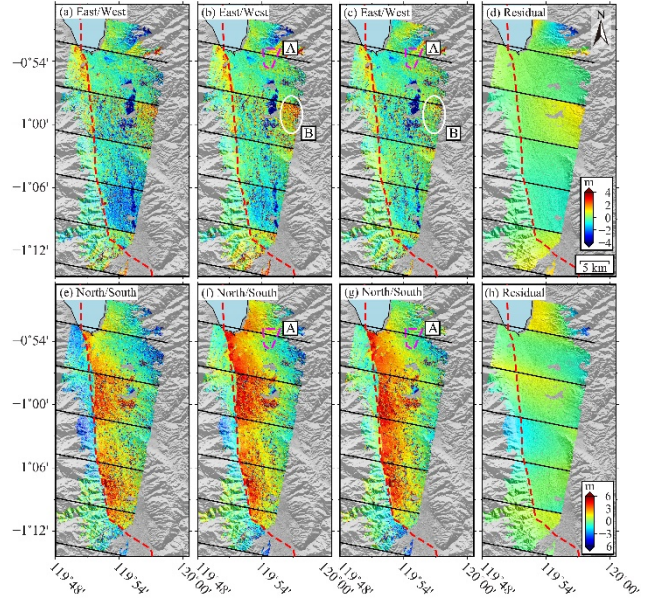
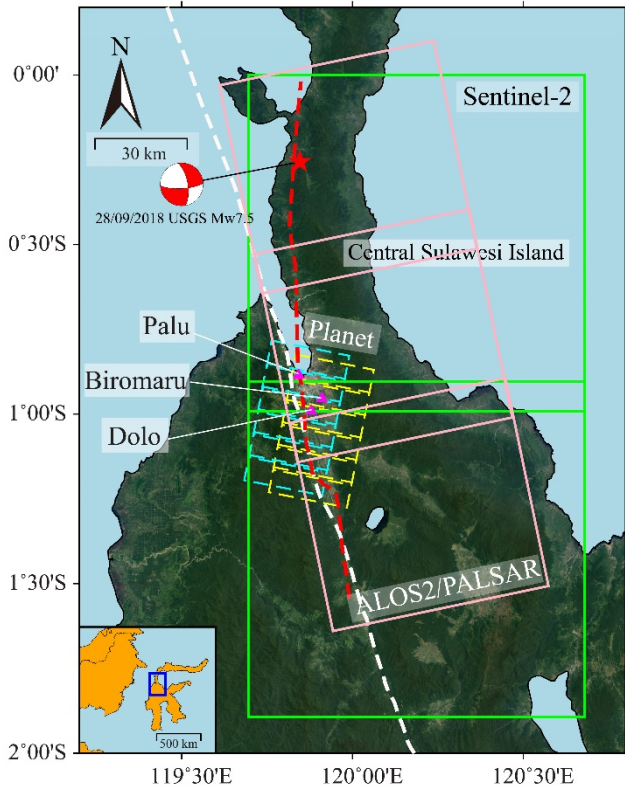


Fig. 4 The offset field obtained from the Planet images after correcting the ramp errors by the full-field method and the proposed block method. (a) and (e) show the original offset fields in the E/W direction and the N/S direction, respectively. (b) and (f) show the offset fields after correcting the ramp errors by the full-field method. (c) and (g) show the offset fields after correcting the ramp errors by the block method. Area A will be used for accuracy assessment in Fig. 5. (d) and (h) show the difference between the results of the two methods. In the figures of this study, east and north offsets are defined as positive values, west and south offsets are negative. The red dotted line indicates the fault line of the Palu earthquake. The black line indicates the block line.

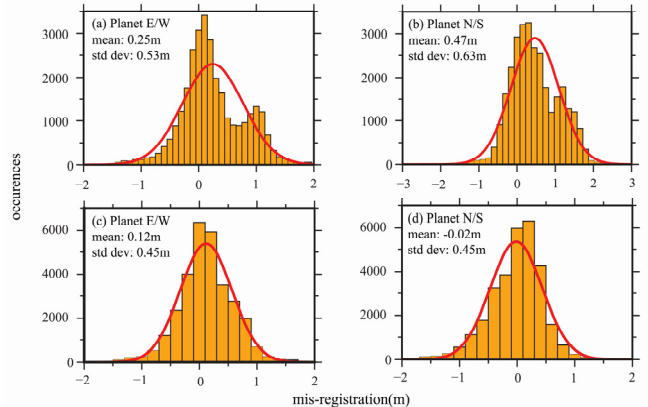


Fig. 5 Statistical histogram of the E/W and N/S offset fields error of the Planet images. (a) and (b) show results of the full-field method in the E/W and N/S directions, respectively. (c) and (d) show the results of the block method in the E/W and N/S directions, respectively.

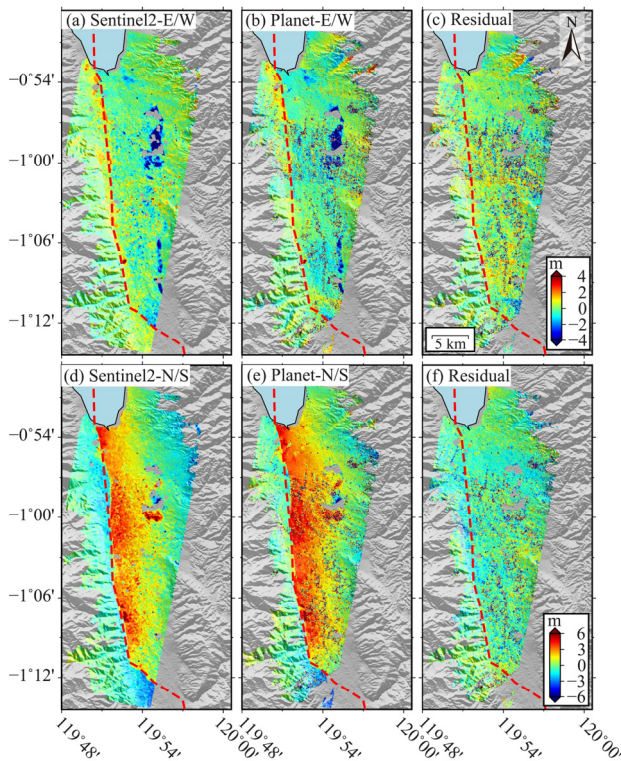


Fig. 6 Offset results extracted from the Planet and Sentinel-2 images. (a) and (d) show the E/W and N/S offsets of the Sentinel-2, respectively. (b) and (e) show the E/W and N/S offsets of the Planet respectively. (c) and (f) are the difference between these two results in the E/W and N/S directions, respectively.

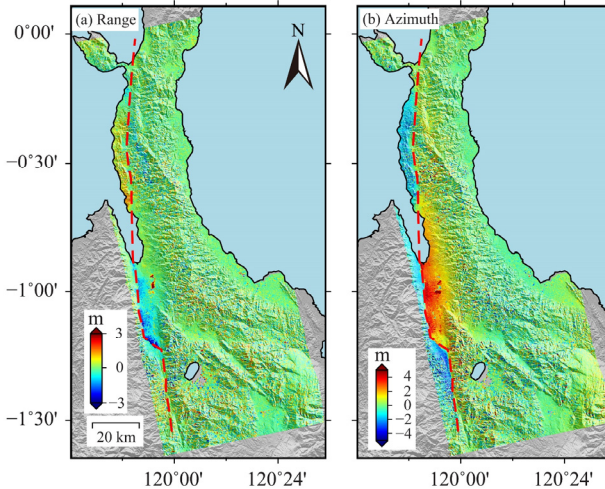


Fig. 7 The (a) range and (b) azimuth deformation results extracted from the ALOS2 images.

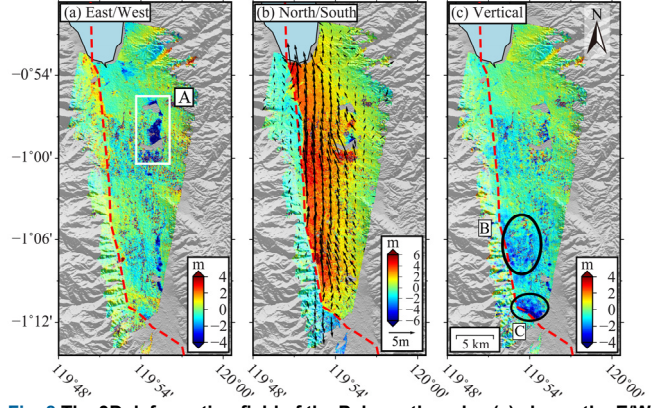


Fig. 8 The 3D deformation field of the Palu earthquake. (a) shows the E/W deformation field. The area outlined by the white frame, area A, represents the landslide area that will be further analyzed in Fig. 9. (b) is the N/S deformation field. The black arrows denote the horizontal displacement vector and the length of the arrow shows the size of the deformation. (c) shows the vertical deformation field. Areas B and C outlined by black circles are the main subsidence areas.

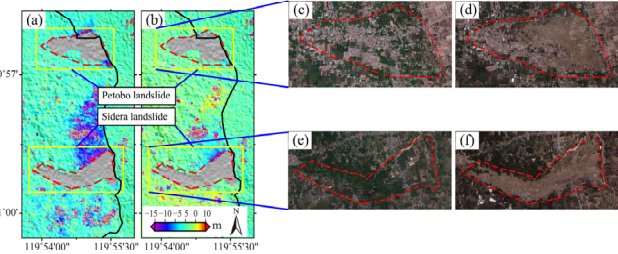


Fig. 9 Offset field of the landslide area. (a) and (b) show the E/W and N/S offset fields of area A in Fig. 8(a), respectively. (c) and (d) are the optical images of Petobo landslide acquired before and after the landslide, respectively. (e) and (f) are the optical images of Sidera landslide acquired before and after the landslide. The red dotted line outlines the area of the landslide. The black solid line indicates the canal.

TABLE 1
OVERVIEW OF OPTICAL SATELLITE PARAMETERS

| Sensors | Planet | | Landsat8 | Sentinel-2 |
|--------------------|---|----------------------------|--|----------------------------|
| Orbit | International Space Station Orbit(ISSO) | Sun-synchronous Orbit(SSO) | Sun-synchronous Orbit(SSO) | Sun-synchronous Orbit(SSO) |
| Orbit Altitude | 400 km(51.6° inclination) | 475 km(~98° inclination) | 705 km(98.2° inclination) | 786 km(98.62° inclination) |
| Images Coverage | 20 km × 12 km | 24.6 km × 16.4 km | 185 km × 185 km | 290 km × 290 km |
| Number Of Bands | 4 bands(Blue, Green, Red, NIR) | | OLI(9 bands including a panchromatic band) and TIRS(2 bands) | 13 bands |
| Spatial Resolution | 3 m | 3.5-4 m | 15 m(panchromatic) | 10 m(NIR) |
| Revisit Period | 1 day | | 16 days | 5 days |

TABLE 2
OPTICAL AND SAR DATA INFORMATION

| Experiments | Sensors | Pre-seismic | Post-seismic |
|----------------------------------|------------|-------------|--------------|
| | | 20180901 | |
| | | 20180911 | |
| Errors analysis and optimal Band | Planet | 20180917 | — |
| | | 20180919 | |
| | | 20180922 | |
| Co-seismic deformation | Planet | 20180927 | 20181001 |
| | Sentinel-2 | 20180917 | 20181002 |
| | ALOS2 | 20180817 | 20181012 |

TABLE 3
PLANET IMAGES DIFFERENT BANDS OFFSETS STANDARD DEVIATION

| | Master-Slave | E/W std dev: (m) | | | | N/S std dev: (m) | | | |
|--|-------------------|------------------|--------------|-------|-------|------------------|--------------|-------|-------|
| | | Band1 | Band2 | Band3 | Band4 | Band1 | Band2 | Band3 | Band4 |
| | 20180901-20180911 | 0.45 | 0.40 | 0.46 | 4.26 | 0.61 | 0.53 | 0.60 | 4.49 |
| | 20180917-20180919 | 0.47 | 0.38 | 0.47 | 4.21 | 0.68 | 0.58 | 0.68 | 4.41 |
| | 20180919-20180922 | 0.55 | 0.45 | 0.52 | 3.72 | 0.71 | 0.55 | 0.67 | 4.05 |

TABLE 4
PARAMETERS FOR OPTICAL IMAGES PROCESSING

| Sensors | COSI-Corr parameters | | | | | NL-means filter parameters | | | |
|------------|-----------------------------------|-----------------------------------|--------------------|----------------------|----------------|----------------------------|-----------------|-----------|-----------|
| Planet | Initial sliding window | Final sliding window | Sliding step size | Number of iterations | Mask threshold | Searching window | Matching window | E/W noise | N/S noise |
| | 64 × 64 pixels (192 m × 192 m) | 32 × 32 pixels (96 m × 96 m) | 5 pixels (15 m) | 2 | 0.9 | 5 × 5 pixels | 3 × 3 pixels | 0.69 | 1.36 |
| Sentinel-2 | 32 × 32 pixels (320 m × 320 m) | 32 × 32 pixels (320 m × 320 m) | 6 pixels (60 m) | 2 | 0.9 | 5 × 5 pixels | 3 × 3 pixels | 0.57 | 0.75 |

ACKNOWLEDGMENT

We thank California Institute of Technology for sharing the COSI-Corr software. We are grateful for the ALOS2 data provided by Japan Aerospace Exploration Agency (JAXA) (PI number: PER2A2N038). We acknowledge the Sentinel-2 data provided by ESA and the Planet optical data provided by the Planet Company. Figures are drawn by the GMT software.

REFERENCES

- [1] S. Leprince, E. Berthier, F. Ayoub, C. Delacourt, and J. P. Avouac, “Monitoring earth surface dynamics with optical imagery,” *EOS, Trans. Amer. Geophys. Union*, vol. 89, no. 1, pp. 1–2, Jan. 2008.
- [2] N. Van Puymbroeck, R. Michel, R. Binet, J.-P. Avouac, and J. Taboury, “Measuring earthquakes from optical satellite images,” *Appl. Opt.*, vol. 39, no. 20, pp. 3486–3494, Jul. 2000.
- [3] S. Leprince, S. Barbot, F. Ayoub, and J.-P. Avouac, “Automatic and precise orthorectification, coregistration, and subpixel correlation of satellite images, application to ground deformation measurements,” *IEEE Trans. Geosci. Remote Sens.*, vol. 45, no. 6, pp. 1529–1558, Jun. 2007.
- [4] M. Taylor, S. Leprince, J. P. Avouac, and K. Sieh, “Detecting coseismic displacements in glaciated regions: An example from the great November 2002 Denali earthquake using SPOT horizontal offsets,” *Earth Planet. Sci. Lett.*, vol. 270, no. 3, pp. 209–220, 2008, DOI: 10.1016/j.epsl.2008.03.028.
- [5] Y. Zhou, et al., “Assessing the ability of Pleiades stereo imagery to determine height changes in earthquakes: A case study for the El Mayor-Cucapah epicentral area,” *J. Geophys. Res. Solid Earth*, vol. 120, no. 12, pp. 8793–8808, 2015.
- [6] J. Hollingsworth, L. Ye, and J. P. Avouac, “Dynamically triggered slip on a splay fault in the Mw7.8, 2016 Kaikoura (New Zealand) earthquake,” *Geophys. Res. Lett.*, vol. 44, pp. 3517–3525, 2017, DOI: 10.1002/2016GL072228.
- [7] A. Käab, B. Altena, and J. Mascaro, “Coseismic displacements of the 14 November 2016 Mw7.8 Kaikoura, New Zealand, earthquake using the Planet optical cubesat constellation,” *NAT HAZARD EARTH SYS*, vol. 17, no. 5, pp. 1–18, 2017.
- [8] G. Hui, S. Z. Li, P. C. Wang, Y. H. Suo, Q. Wang, and I. D. Somerville, “Linkage between reactivation of the sinistral strike-slip faults and 28 September 2018 Mw7.5 Palu earthquake, Indonesia,” *SCI BULL*, vol. 63, no. 24, pp. 1635–1640, 2018.

- [9] Planet Team, "Planet imagery product specifications, Planet," San Francisco, CA, USA, 2019. [Online]. Available: <https://assets.planet.com/docs/combined-imagery-product-spec-final-may-2019.pdf>.
- [10] F. Ayoub, S. Leprince, and J.P. Avouac, "User's Guide to COSI-CORR Co-registration of Optically Sensed Images and Correlation," Jun. 2017. [Online].
- [11] A. Stumpf, D. Michéa, and J. P. Malet, "Improved Co-Registration of Sentinel-2 and Landsat-8 Imagery for Earth Surface Motion Measurements," *Remote Sens.*, vol. 10, no. 2, pp. 160, 2018.
- [12] A. Buades, B. Coll, J.-M. Morel, "Nonlocal image and movie denoising", *Int. J. Comput. Vis.*, vol. 76, no. 2, pp. 123-140, 2008.
- [13] A. Socquet, J. Hollingsworth, E. Pathier, and M. Bouchon, "Evidence of supershear during the 2018 magnitude 7.5 Palu earthquake from space geodesy," *Nat. Geosci.*, vol. 12, pp. 192-199, 2019.
- [14] X. G. Song, Y. F. Zhang, X. J. Shan, Y. H. Liu, W. Y. Gong, and C. Y. Qu, "Geodetic observations of the 2018 Mw 7.5 Sulawesi earthquake and its implications for the kinematics of the Palu fault," *Geophys. Res. Lett.*, vol. 46, pp. 4212-4220, 2019.
- [15] H. Takagi, M. B. Pratama, S. Kurobe, M. Esteban, R. Aránguiz, and B. Ke, "Analysis of generation and arrival time of landslide tsunami to Palu City due to the 2018 Sulawesi Earthquake," *Landslides*, vol. 16, no. 5, pp. 983-991.
- [16] L. J. He, G. C. Feng, Z. W. Li, Z. X. Feng, H. Gao, and X. X. Wu, "Source parameters and slip distribution of the 2018 Mw 7.5 Palu, Indonesia earthquake estimated from space-based geodesy," *Tectonophysics*, vol. 772, 2019.
- [17] O. Bellier, M. Sébrier, D. Seward, T. Beaudouin, M. Villeneuve, and E. Putranto, "Fission track and fault kinematics analyses for new insight into the Late Cenozoic tectonic regime changes in West-Central Sulawesi (Indonesia)," *Tectonophysics*, Vol: 413, pp: 201-220, 2006.
- [18] M. Drusch et al., "Sentinel-2: ESA's optical high-resolution mission for GMES operational services", *Remote Sens. Environ.*, vol. 120, pp. 25-36, May 2012.
- [19] L. J. He, G. C. Feng, Z. X. Feng, and H. Gao, "Coseismic displacements of 2016 Mw7.8 Kaikoura, New Zealand earthquake, using Sentinel-2 optical images," *Acta Geodaetica et Cartographica Sinica.*, vol. 48, no. 3, pp. 339-351, 2019, DOI: 10.11947/j.AGCS.2019.20170671.
- [20] C. Werner, U. Wegmüller, T. Strozzi, and A. Wiesmann, "Gamma SAR and interferometric processing software," in *Proc. ERS-ENVISAT Symp., Gothenburg, Sweden*, 2000, pp. 16-20. [Online]. Available: <http://citeseerx.ist.psu.edu/viewdoc/download?doi=10.1.1.20.6363&rep=rep1&type=pdf>.
- [21] J. H. Liu, J. Hu, Z.-W. Li, J. J. Zhu, Q. Sun, and J. Gan, "A method for measuring 3-D surface deformations with InSAR based on strain model and variance component estimation," *IEEE Trans. Geosci. Remote Sens.*, vol. 56, no. 1, pp. 239-250, Jan. 2018.
- [22] G. C. Feng, B. Xu, X. J. Shan, and G. H. Zhang, "Coseismic deformation and source parameters of the 24 September 2013 Awaran, Pakistan Mw7.7 Earthquake derived from optical Landsat8 satellite images," *Chinese J. Geophys.*, vol. 58, no. 5, pp. 1634-1644, 2015, DOI: 10.6038/cjg20150515.
- [23] Y. S. Zhou, J. Hu, Z. W. Li, J. Li, R. Zhao, and X. L. Ding, "Quantifying glacier mass change and its contribution to lake growths in central Kunlun during 2000–2015 from multi-source remote sensing data," *J. HYDROL.*, vol. 570, pp. 38-50, 2019.
- [24] D. Scherler, S. Leprince, and M. R. Strecker, "Glacier-surface velocities in alpine terrain from optical satellite imagery—Accuracy improvement and quality assessment," *Remote Sens. Environ.*, vol. 112, no. 10, pp. 3806– 3819, Oct. 2008.
- [25] C. Ding, G. C. Feng, Z. W. Li, X. J. Shan, Y. N. Du, and H. Q. Wang, "Spatio-Temporal Error Sources Analysis and Accuracy Improvement in Landsat 8 Image Ground Displacement Measurements," *Remote Sens.*, vol. 8, no. 11, pp. 937, 2016, DOI: 10.3390/rs8110937.
- [26] S. Leprince, "Monitoring Earth Surface Dynamics with Optical Imagery," Ph.D. dissertation, Dept. Elect. Eng., Caltech., Pasadena, California, USA, 2008.
- [27] M. Necsoiu, S. Leprince, D. M. Hooper, C. L. Dinwiddie, R. N. McGinnis, and G. R. Walter, "Monitoring migration rates of an active subarctic dune field using optical imagery," *Remote Sens. Environ.*, vol. 113, no. 11, pp. 2441–2447, Nov. 2009.
- [28] S. Leprince, F. Ayoub, Y. Klinger, and J. P. Avouac, "Co-registration of optically sensed images and correlation (COSI-Corr): An operational methodology for ground deformation measurements," in *Proc. IGARSS*, Barcelona, Spain, Jul. 2007, vol. 6, pp. 1943–1946.